# Magnetohydrodynamics and particle-in-cell codes simulation of plasma processes in micro HEMP-Thrusters

**IEPC-2013-145**

*Presented at the 33$^{rd}$ International Electric Propulsion Conference,*
*The George Washington University, Washington, D.C., USA*
*October 6–10, 2013*

Tim Brandt[1,3,*], Rodion Groll[2] , Frank Jansen[1],
Ulrich Johann[4] , Andreas Keller[4,5],
Holger Kersten[3], and Claus Braxmaier[1,2]

[1] *DLR, Institute of Space Systems, Robert-Hooke Str. 7, 28359 Bremen, Germany*
[2] *ZARM, University of Bremen, Am Fallturm, 28359 Bremen, Germany*
[3] *Christian-Albrechts-Universität zu Kiel, Plasma Technology Group, Leibnizstraße 19, 24098 Kiel, Germany*
[4] *Astrium GmbH, Claude-Dornierstraße* 1, 88090 *Immenstaad, Germany*
[5] *Justus-Liebig-University Gießen, I. Physikalisches Institut*

**Abstract: In this work concepts for numerical simulation with the aim of improved understanding of a miniaturized HEMP (High Efficiency Multistage Plasma) Thruster are presented. A downscaled HEMP-Thruster is developed at Astrium GmbH at Friedrichshafen in cooperation with the Center of Applied Space Technology and Microgravity (ZARM) and the German Aerospace Center (DLR). The aim is to reach the low thrust level and noise of the requirement for LISA (Light Interferometer Space Antenna) and similar formation flight space missions. With a complete model of the thruster and its environment, it should be possible to optimize characteristics like thrust beam divergence, thrust weight ratio and power consumption, as well as to determine if and how the LISA requirements can be met. Both an analytical and a particle model for calculating the electron confinement in the complex magnetic field topology are presented. A simplified fluid model gives first estimations of plasma density and electron temperature. Information about plasma potential and ring currents through E $\times$ B drift is gathered. Comparison of the results of the different models are drawn.**

## Nomenclature

| | |
|---|---|
| $HEMPT$ | = High Effciency Multistage Plasma Thruster |
| $PIC$ | = particle-in-cell |
| $e$ | = electron charge |
| $m_e$ | = electron mass |
| $\boldsymbol{v}$ | = particle velocity vector |
| $\boldsymbol{E}$ | = electric field vector |
| $\boldsymbol{B}$ | = magnetic field vector |

[*] *Corresponding author email address: tim.brandt@dlr.de*

# I. Introduction

Upcoming formation flying missions like LISA have never before seen requirements for low thrust ($0,1$ µN region) with little noise (lower than a spectral resolution of $0,1$ µN/$\sqrt{\text{Hz}}$ can resolve), but also for long lifetime and fuel as well as energy efficiency. The High Efficiency Multistage Plasma Thruster patented by Thales has already shown the later characteristics.[1] Simplicity of design is the guiding theme of this type of thruster.[2] Its discharge chamber is a simple cylinder with an open end. Ring shaped periodically poled permanent magnets create several dipolar cusps (Fig. 1). This magnetic field structure leads to low erosion of the discharge chamber inner walls.[3] Electron confinement is archived through magnetic mirroring and $\mathrm{E} \times \mathrm{B}$ drift near the cusps. Additionally, a relatively large number of electrons are confined outside the discharge chamber near its exit. These create a negative space charge that allows for ion acceleration without use of grids, which are known to be prone to erosion.[4] With the neutralizer cathode near the exit being grounded, and an anode at the closed end of the discharge chamber, this allows for ionization by electron collisions and acceleration of the ions through the same electric field, improving the efficiency.[5]

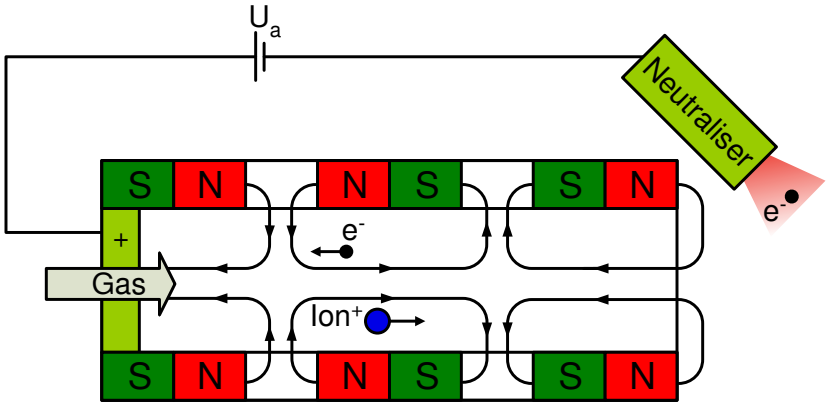


**Figure 1. HEMP-Thruster principle[6]**

In an attempt to use these properties for low thrust, at Astrium GmbH in Friedrichshafen in cooperation with the Center of Applied Space Technology and Microgravity (ZARM) and the German Aerospace Center (DLR), a downscaled HEMP-Thruster has been developed. This so called micro HEMP-Thruster has undergone an intensive measurement campaign. First results are promising.[6] To finally reach the low thrust as well as the low noise, a better understanding of the plasma inside the thruster and near its exit is required. Since the small size of the discharge chamber prohibits invasive measurement, computer modeling is one of the few options left. For this both particle as well as fluid simulation are considered.

For the PIC simulation the VORPAL engine[7] from TECH-X is used. The fluid simulation is performed by use of the plasma module of the COMSOL Multiphysics Software. Magnetic field for both fluid and particle simulation is calculated by the so called AC-DC- module of the same software package. Distribution of gaseous neutrals is calculated by use of OpenFOAM.

While particle simulations are believed to produce more accurate results, they are noisy by nature, possibly dominating over the real noise of the plasma. Thus, a fluid particle hybrid code is considered, by using the accuracy of the movements of electrons from the particle code, and the ions as a fluid, whereas later smooths the overall result. In preparation for this attempt, here several simplified models are presented, to test the used codes under the conditions of the micro HEMPT as well as to get first results about the function of this thruster.

# II. Theory

## A. Electron gyration movement

For modeling magnetized plasma like in the discharge chamber of the micro HEMPT, we shall briefly recall the principal effects of the magnetic field on charged particles.

An electrically charged particle (electron), in external magnetic and electric fields experiences the Lorentz-force:

$$\boldsymbol{F} = m_e \cdot \frac{d\boldsymbol{v}}{dt} = e(\boldsymbol{E} + \boldsymbol{v} \times \boldsymbol{B}) \tag{1}$$

In a case without electric field, and where for simplicity of calculation a Cartesian coordinate system shall be oriented such that its $z$-axis is parallel to the magnetic field $B$, the Lorentz-force causes a gyration of the electron with the gyration radius

$$r_L = \frac{v_\perp m_e}{eB} \quad , \tag{2}$$

and the gyration frequency:

$$\omega_g = \frac{eB}{m_e} \quad , \tag{3}$$

where $v_\perp$ is the electrons velocity component perpendicular to the magnetic field. Further, its parallel component $v_{||}$ remains unaffected, so its center of gyration moves parallel to the magnetic field. The gyration motion means that large scale motions of the electron perpendicular to the magnetic field are prohibited. Its center of gyration does not only follow straight, but also curved field lines, under the condition that its gyration radius is much smaller than that curvature.

### B. E × B drift

In a magnetized plasma, both magnetic and electric fields act upon the charged particles. If the electric field has a component perpendicular the magnetic field, un-intuitive movement of the electron occurs. Under the same coordinate system alignment as in the example before, there shall be an $E_x$ component ($E_y$ component and combination of both would work as well). Only the $x$-$y$-plane shall be investigated, meaning that the $v_{||}$ movement is ignored. When during its gyration the electron moves into the direction of the electric field, it accelerates and its radius of gyration becomes larger, and opposed to it this radius becomes smaller. Therefore, on average, its center of gyration moves into the $y$-direction with the speed[8] :

$$\boldsymbol{v_d} = \frac{\boldsymbol{E} \times \boldsymbol{B}}{\boldsymbol{B}^2} \quad . \tag{4}$$

The obvious characteristic of this motion is that it is perpendicular both to the magnetic and the electric field, hence it is called E × B drift.

### C. Magnetic mirror

The dipolar cusps of the HEMPTs magnetic field configuration makes use of the so called mirror effect.

This effect can be described by use of a magnetic moment of an electron in a magnetic field which can be expressed as:

$$\mu = \frac{0.5 m v_\perp^2}{B} \quad . \tag{5}$$

If no other forces than magnetic ones are acting upon the electron, it can be assumed that the magnetic moment and the kinetic energy does not change.[9] This is called the adiabatic invariance of the magnetic moment. When an electron moves into a region with denser field, $B$ and $v_\perp^2$ raises and therefore $v_{||}^2$ has to drop for the kinetic energy to remain constant. $v_{||}^2$ finally reaches zero. At this point $v_{||}$ changes its sign and $v_{||}^2$ rises again as the electron moves back into the weaker field so $B$ drops again.[10]

The actual reason for this behavior can be understood by considering that increasing magnetic density means converging field lines. Since an electron moves through the nearby surroundings of the field line due to gyration, it experiences a magnetic component perpendicular to the direction of that line. This perpendicular component causes a component of the Lorentz force parallel to its line and, therefore, also parallel to $v_{||}$. So this is an acceleration force that drives the electron out of the region with denser magnetic field. An electron can become trapped in a region with weak field that lies between two regions with denser field, if the field line it is following goes through these two regions. Based on the analytical description through the magnetic moment, for an electron a mirror ratio can be expressed as: $M_R = B_{max}/B_{min}$ and electrons that meet the following criteria are reflected:

$$\frac{v_\perp}{v_{||}} > -\frac{1}{\sqrt{M_R}} \qquad . \tag{6}$$

The electrons have a pitch angle to that field line which is defined as $tan\Theta = v_\perp/v_{||}$. According to this criteria, electrons with a small pitch angle are not reflected. These are said to be in the loss cone.

### D. Particle-in-cell method

Most simulation models presented here make use of a particle-in-cell code, which makes use of a particle approach for plasma simulation.

Each electron and ion is a source of an electric field due to its charge and the source of magnetic field due to its motion. The cheer number of charged particles in real world plasma would make calculation even on computer clusters impossible. Hoverer, it has been shown that basic behavior of plasma does not change, when thousands of particles are summed up to macro particles.[11] This brings the number of particles to a manageable size. Number of calculations can still be extremely high, considering that for every single particle its interactions through electric and magnetic fields with every other particle must be calculated for each time step. Thus, the so called particle-in-cell codes apply a grid to the simulation domain, with a resolution such that on average several particles are in each cell of the grid. The particle charges and movements, later in form of electric currents, are summed up to the nearest four grid points, with a weighting according to their distance from the grid points. From these findings the electric and magnetic fields are calculated. Then for each electron the Lorentz-force is applied, with the same weighting of the fields regarding the grid points distances like before for the charges and currents. The electrons are moved concerning to the velocity they already had, their acceleration is by the Lorentz-force (which is dependent on that velocity). After a time step new positions and velocities of the particles are observed and the cycle is repeated.

This method can approximate the behaviors of plasma well.[12] Close distance interactions of charged particles are neglected, but this can be compensated by use of Monte Carlo collisions.[13] Usually, the performance of particle-in-cell codes is improved, for example by using leap frog method[14] for progressing in simulated time or by using second order interpolation for the weighting.[15]

### E. Equations for a fluid plasma model

The other widely used method for simulating plasmas is the fluid approach.

The fluid model in chapter III E describes the rate of change in electron density $n_e$ by drift diffusion equitation:[16]

$$\frac{\partial}{\partial t}(n_e) + \nabla \cdot \Gamma_e = R_e \qquad , \tag{7}$$

where $R_e$ is the sum of sources and sinks of the electrons. The electron flux $\Gamma_e$ is defined as:

$$\Gamma_e = -n_e(\boldsymbol{\mu_e} \cdot \boldsymbol{E}) - \boldsymbol{D}_e \cdot \nabla n_e \qquad . \tag{8}$$

On the right side of the equation, the first term describes the movement of the electrons caused by the electric field by use of the electron mobility $\boldsymbol{\mu_e}$, while the second term describes the diffusion by use of the

electron diffusion coefficient $D_e$, which is related to the mobility by Einstein's relation. Since here a magnetic field is applied, the mobility becomes a tensor, which inverse can be written in compact form as:

$$\boldsymbol{\mu_e^{-1}} = \mu_{e0}^{-1} \begin{pmatrix} 1 & -\mu_{e0}B_z & 0 \\ \mu_{e0}B_z & 1 & -\mu_{e0}B_r \\ 0 & \mu_{e0}B_r & 1 \end{pmatrix} \quad , \tag{9}$$

with the quantity $\mu_{e0}$ being the scalar electron mobility in the absence of a magnetic field, and the magnetic field components $B_z$, $B_r$, $B_{phi}$ (which are calculated as described in the following chapter, II F ). The mobility is several magnitudes lower perpendicular to the magnetic field then parallel to it. This concurs with the electrons gyration around the magnetic field lines as described in chapter II A. The electron mobility perpendicular to the magnetic field is none-zero due to collisions.[17] The multiplication of the mobility tensor with the electric field vector accounts for the $E \times B$ drift described in chapter II B. The magnetic mirror force described in chapter II C is not accounted for.

The electron energy density $n_\epsilon$ is given in a similar fashion like the drift diffusion equation:[18]

$$\frac{\partial}{\partial t}(n_\epsilon) + \nabla \cdot \Gamma_\epsilon + E \cdot \Gamma_e = R_\epsilon \quad . \tag{10}$$

The term $E \cdot \Gamma_e$ accounts for the energy gain or loss of the electrons in the electric field. $R_\epsilon$ is the energy loss/gain due to inelastic collisions. The energy flux density is

$$\Gamma_\epsilon = [-n_\epsilon(\boldsymbol{\mu}_\epsilon \cdot \boldsymbol{E}) - \boldsymbol{D}_\epsilon \cdot \nabla n_\epsilon] \quad . \tag{11}$$

The electron energy mobility $\boldsymbol{\mu}_\epsilon$ is directly proportional to the electron mobility:[18]

$$\boldsymbol{\mu}_\epsilon = \frac{5}{3}\boldsymbol{\mu}_e \quad . \tag{12}$$

The change of the Xenon-ion density $n_{\mathrm{Xe}}$ is also described by a drift diffusion equation:

$$\frac{\partial}{\partial t} n_{\mathrm{Xe}} + \boldsymbol{\nabla} \cdot (n_{\mathrm{Xe}} \boldsymbol{\mu}_{\mathrm{Xe^+}} \boldsymbol{E} - \boldsymbol{D}_{\mathrm{Xe^+}} \boldsymbol{\nabla} n_{\mathrm{Xe}}) = R_{\mathrm{Xe^+}} \quad . \tag{13}$$

The diffusion tensor of the ions $\boldsymbol{D}_{\mathrm{Xe^+}}$ is calculated via Einstein relation from the ion mobility, by use of the mobility tensor $\boldsymbol{\mu}_{\mathrm{Xe^+}}$.

The sources and sinks for the electrons and ions, $R_e$, $R_{\mathrm{Xe^+}}$, as well as the sources and sinks for the electron energy $R_\epsilon$, are described by reactions on the surface and in the plasma volume. Reactions in the volume are the collisional ionization of unexcited neutral xenon: $e + Xe => 2e + Xe^+$. This reaction obviously serves as a source for both electron and ions, and as a sink for energy by 12.12 eV per reaction. This is a very simplified plasma model, no excitation, superelastic collisions and ionization of exited ions is included. Elastic collisions, $e + Xe => e + Xe$, are included, they do not change the energy or particle density, but the direction of the "fluid" streams. Surface reactions are absolute sinks for electrons and ions by neutralization, $Xe^+ => Xe$ , and by being absolutely absorbing for electrons.

With the exception of the anode surface, the inner walls of the discharge chamber are dielectrics. Therefore, surface charge ($\rho_{surf}$) accumulation is accounted by:

$$\frac{\partial}{\partial t}\rho_{surf} = J_e \cdot J_{Xe^+} \quad , \tag{14}$$

with $J_e$ being the electron current normal to the surface, and $J_{Xe^+}$ being the ion current normal to the surface.

The distribution of the neutral Xe is calculated in a different fluid simulation described in chapter III A and the result is used as a static background.

Finally, the electric potential $\Phi$, from which the electric field $\boldsymbol{E}$ is derived, is calculated by the electron and ion densities due to Poisson's equation:

$\epsilon_0 \epsilon_r \Delta\Phi = n_e + n_{\mathrm{Xe}}$ .

### F. Modeling a magnetic field

The magnetostatic field created by the permanent magnets was simulated by use of finite element method. The magnetization $\boldsymbol{M}(\boldsymbol{r})$ is the source of the magnetic field in their domains via $\boldsymbol{B}(\boldsymbol{r}) = \mu_0 \boldsymbol{M}(\boldsymbol{r})$. For the remaining simulation domain Gauss law of magnetism, $\boldsymbol{\nabla} \cdot \boldsymbol{B}(\boldsymbol{r}) = 0$, is applied. The solver makes use of the scalar potential $V_{\mathrm{m}}$ with $\boldsymbol{B}(\boldsymbol{r}) = -\mu_0 \boldsymbol{\nabla} V_{\mathrm{m}}(\boldsymbol{r})$.

## III. Model setup

### A. Finite volume simulation of the neutral gas

Knowledge of the neutral gas distribution is essential for accurately calculating the spatial dependent ionization rate (applied in chapter III E)

For the neutral gas simulation, a finite volume method fluid simulation was performed. Under consideration of the cylinder geometry of the micro HEMP-Thruster, the simulation was performed only in the $r$-$z$-plane. To incorporate the volumina streams, the thickness of this plane is chosen to be non-zero. This is a so called 2.5 d type of simulation. In accordance with the measurement conditions, a gas inlet stream of 0.5 sccm was applied.

### B. Magnetic field model

Obviously, a precise knowledge of the magnetic field is needed. Due to the small size of the micro HEMPTs discharge chamber a Hall probe measurement is practically impossible. Therefore, knowledge of the field data can only be obtained through computer modeling.

Like the neutral gas distribution model the applied model makes use of the cylinder geometry. However, here the thickness of the $r$-$z$ plane is really zero, making it a true 2 d simulation. This scheme is also applied to all plasma simulation models described in the following chapters saving vast amounts of computing power.

Here, this assumption simplifies the magnetic rings to rectangular domains, without diminishing the accuracy of the result. The permanent magnets have a magnetization of $M = 724$ kA/m in the $z$-direction.

### C. An analysis of the electron reflection

The confinement of the electrons by the magnetic field is of special interest, since better confinement can increase the plasma density and, therefore, thruster performance.

Along with being bound to follow the magnetic field lines, confinement is achieved by the reflection through the mirror effect.

The reflection probability for an electron generated at each position can be calculated by using the reflection criteria (chapter II C, Eq. 6). Therefore, from each position the magnetic field lines are followed in both directions, and along the field line the maximum magnetic field strength $B_{max}$ is determined.

An uniform angle distribution for the initial velocity vector of the particles is assumed. A hemisphere, which consists of all possible velocity vectors, is than oriented according to the magnetic field line. Figure 2 shows a cross section of that hemisphere. In the green area are the electrons which are reflected, the white area stands for the loss cone. Thus, the relative number of reflected particles can be calculated. While with this method calculation can be made for any point, obviously, a non-infinite number of points must be chosen. Points in a rectangular grid of 0.02 mm distance are selected. The magnetic field is imported from the static magnetic field simulation described in chapter III B.

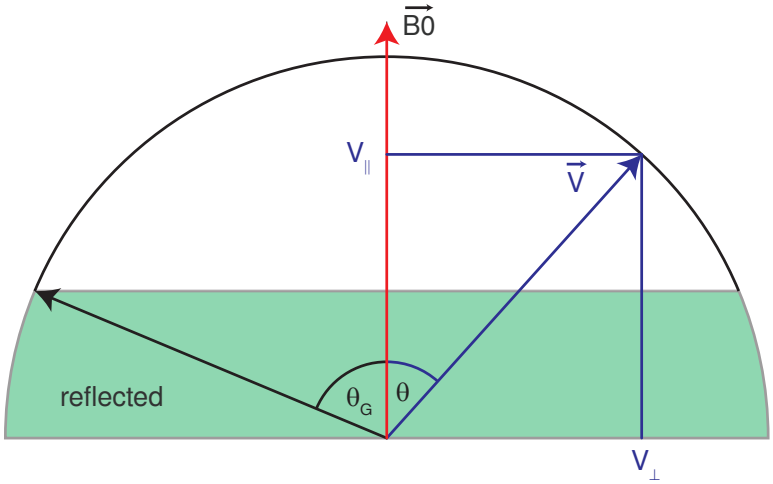


**Figure 2. Nomenclature of the hemisphere used for calculating the electron refection probability.**

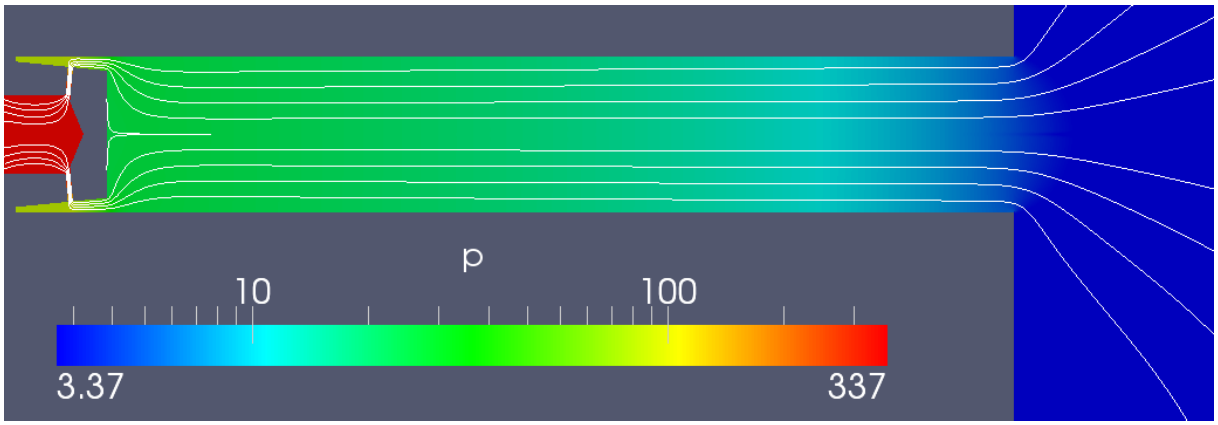


**Figure 3. Pressure distribution (Pa) of a rotational symmetric neutral gas simulation, velocity direction as streamlines.**

### D. A numeric simulation of the electron reflection

A particle-in-cell simulation is performed in an attempt to compare the actual confinement of the electrons with the idealized analytical prediction. In order to match the conditions of the analysis the background electric potential is set to zero, and electrons are defined to have no influence to the potential. So no electric field acts on any of the electrons. The magnetic field is taken again from the results of the model described in chapter III B, with a high resolution of 0.02 mm. This is due to the necessity of taking into account a magnetic field component perpendicular to $v_{||}$, as mentioned in the description of the mirror force in chapter II C. The resolution of the magnetic field must be in the order of magnitude of the gyration radius of the electron, for the changes in that perpendicular component to be applied correctly. While for the analytical method in chapter II C the gyration radius and therefore the magnitude of the velocity vector was irrelevant, here the movement of the electrons is traced, and therefore both the initial velocity magnitude and direction must be given. This is here achieved by a random generator that gives an average thermal velocity of 10 eV, a value that is orientated on measurements in the plasma plume. Like in the analytical simulation, the domain is of the size $r_{Max} = 17$ mm and $z_{Max} = 27,5$ mm. The domain is filled with electrons, except for positions larger than $r = 1,5$ mm up to $z = 17,5$ mm. The time steps are $5 \cdot 10^{-12}$ s, to sufficiently resolve the gyration motion. The simulation is performed over 20000 time steps.

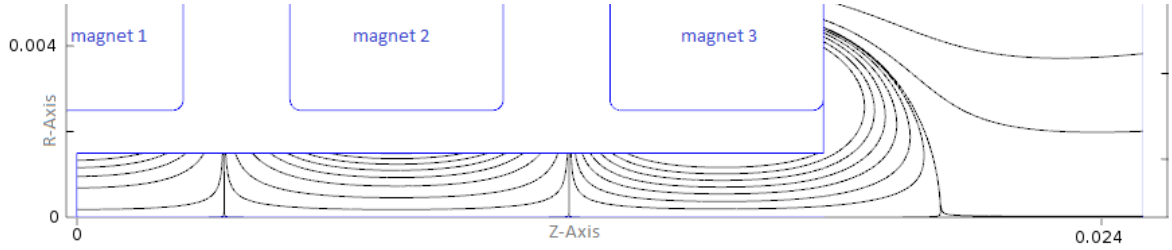


**Figure 4. Streamline plot of the magnetic field in the free space in the HEMPT and its surrounding.**

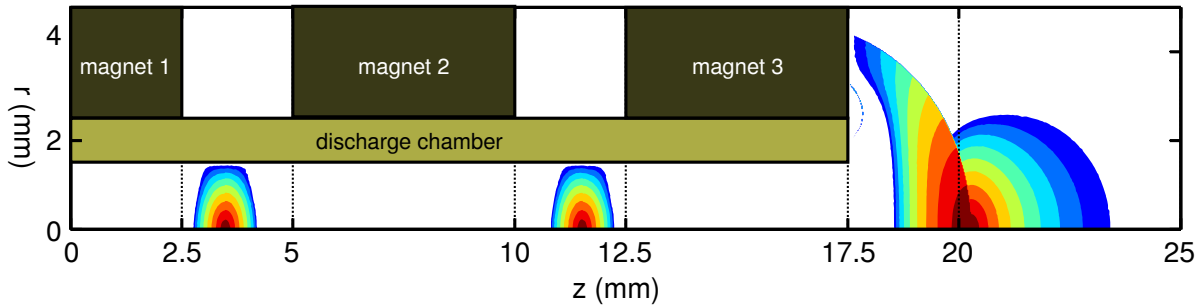


(a) Trapping probability of electrons as contour plot. The filled contour areas rise in steps of 0.1 up to 1.

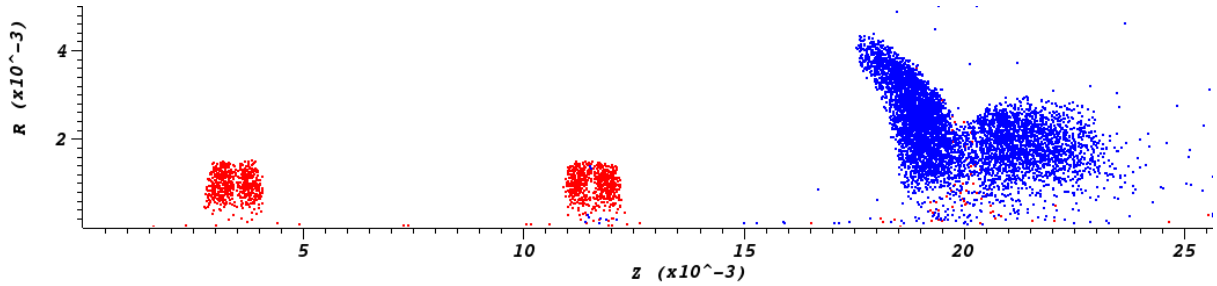


(b) Distribution of the macro-electrons after movement in the magnetic field of the micro HEMP-Thruster for 20000 time steps ($1 \cdot 10^{-7}$ s). Electrons originating inside the discharge chamber colored red, electrons originating outside colored blue.

**Figure 5. Comparison of analytic calculation and numerical simulation**

### E. Fluid model of the plasma

While it has some drawbacks like of not taking into account the mirror force, and being inappropriate for the thruster plume, a fluid plasma model can give a first estimation of the plasma density and structures with relatively little use of computing time.

In this fluid model an anode potential is ramped up from 0 V to 100 V within the simulation time, which is $1 \cdot 10^{-8}$ seconds. It is separated into 100 time steps. This simulation is not intended to reach steady state. Most notably it has no restriction for anode current. Therefore, continuing for much longer times would result in extraordinary high plasma densities. The result for the last time step for the neutral gas simulation described in chapter III A is taken as a stationary neutral gas distribution (Fig. 3). It is idealized and approximated with a mathematic function: $14 * cos(z * pi/0.024) + 16$. Initial electron density is set to $1 \cdot 10^{16}$ particles per cubic meter. Simulation does not include a neutralizer as an electron source. It is assumed that for the short time span of the simulation, the electrons from the plasma outside the discharge chamber will suffice. The electron mobility (a component of the magnetic field dependent conductivity tensor) is defined as $1 \cdot 10^{25}/n_g$, with $n_g$ being the neutral gas density in particles per cubic meter.

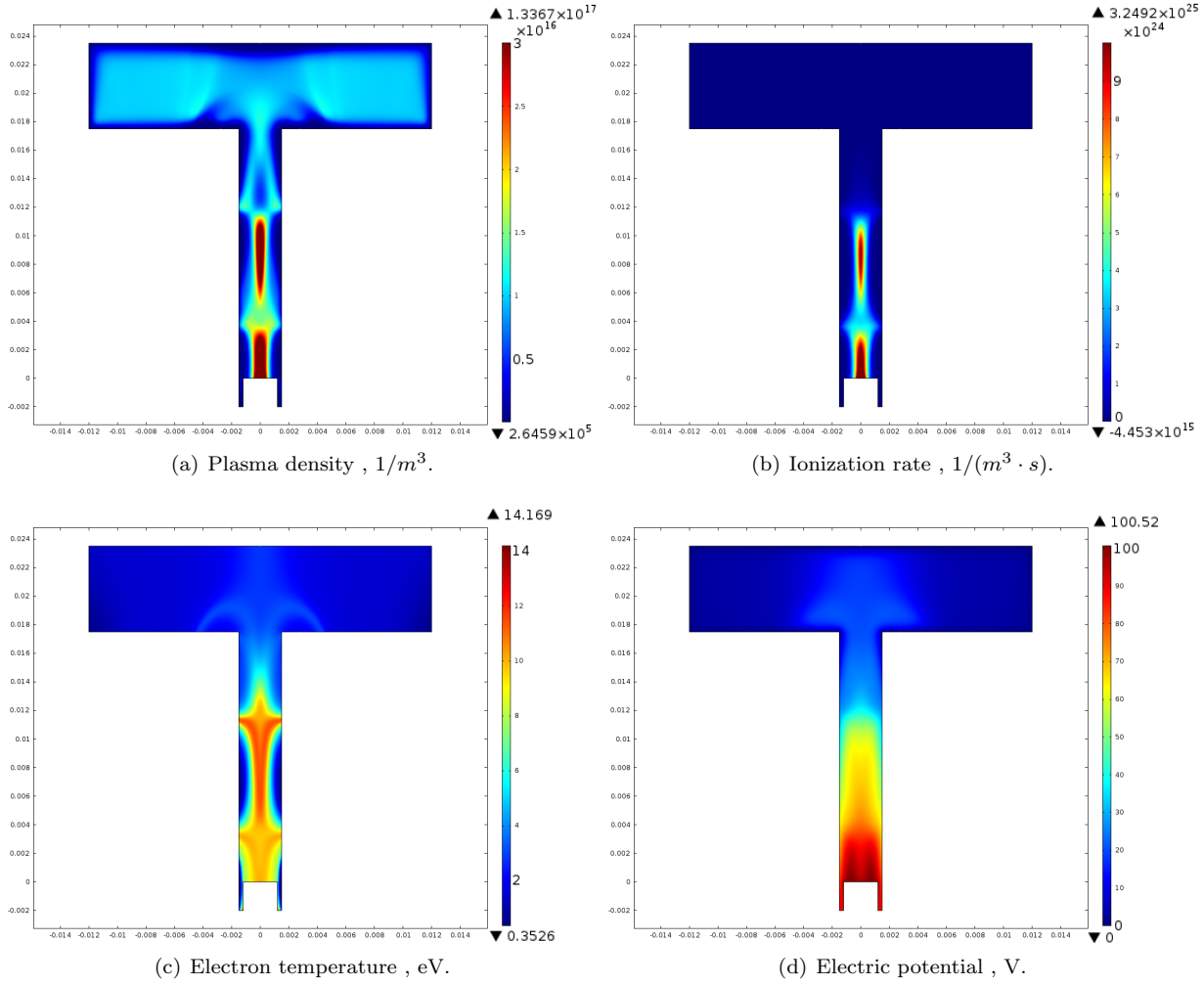


(a) Plasma density , $1/m^3$.

(b) Ionization rate , $1/(m^3 \cdot s)$.

(c) Electron temperature , eV.

(d) Electric potential , V.

**Figure 6. Plasma parameters after $1 \cdot 10^{-8}$ seconds.**

## F. Model of electrons near the cusp

The anode voltage included in the fluid plasma model will consequently result in a potential drop towards the exit. It is believed that the potential drop occurs in steps near the cusps, which have their cause in the hindering of movement of the electrons near the cusps. A particle model of the environment of a cusp is set up to further investigate this.

Domain of this model is $r = 0..1.5$ mm and $z = 0..7.5$ mm. The cusp is at $z = 3.75$ mm. From now on, all positions with $z$-values smaller than 3.75 mm shall be called left to the cusp, and all with bigger values right to the cusp. Following the analytical consideration, that its center of gyration follows a magnetic field line, no electron should be able to move from a position right to the cusp to a position left to the cusp and vice versa. The sole exception would be an electron for which the center of gyration is positioned exactly on the $z$-axis. Yet because at the $z$-value of the cusp and at $r$=0, the magnetic field is zero and close to zero nearby the gyro radius is not negligible anymore. This can lead to chaotic trajectories, as described in Ref.[19] As a result the electrons can pass the cusp in the $z$-direction. In this model the electron current has a value of 10 mA, which is a common value for the micro HEMP-Thruster under investigation. As source of this current, $6.24 \cdot 10^{16}$ electrons per second are generated in a small volume near the right end of the simulation domain. A time step of this simulation is $1 \cdot 10^{-12}$ s, so there are $6.24 \cdot 10^4$ electrons generated per time step. Initial thermal energy of the electrons is again set to be 10 eV. For this relatively simple study, from the three magnetic rings, only the two necessary to generate one cusp are simulated, hence the magnetic

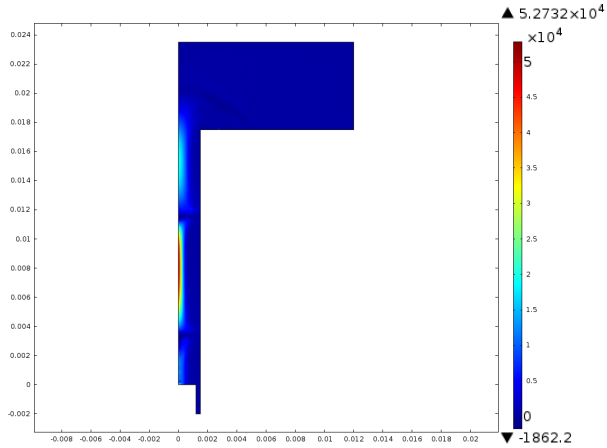


(a) Electron current density , $A/m^2$, z-component.

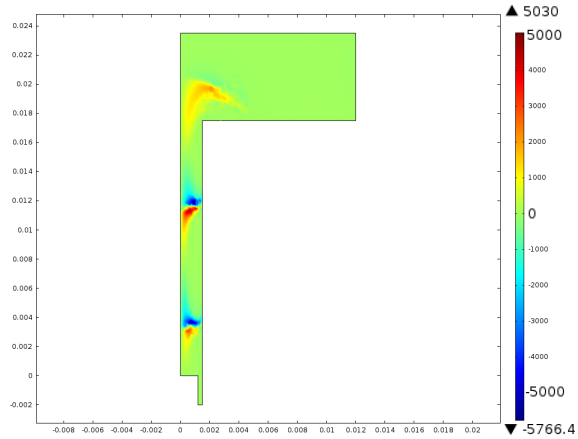


(b) Electron current density , $A/m^2$, r-component.

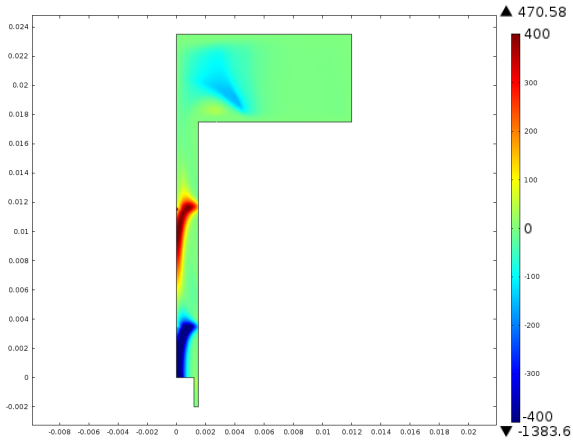


(c) Electron current density , $A/m^2$, phi-component.

**Figure 7. Electron current densities after $1 \cdot 10^{-8}$ seconds.**

field is absolutely symmetric to the $z$-position 3.75 mm. Magnetic field calculation is performed in the same way as in chapter III B. For this very schematic model, a constant electric field into $z$- direction is applied. The resulting linear potential drop is from 166.7 V to 0 V. Typical value of the anode potential is 500 V. Since three potential steps are assumed (each one at the two cusps and one at the discharge chamber exit), one third of this value is taken. Most recent simulations of HEMP-Thrusters show the potential drop at the chamber exit being by far the largest.[20] Without further investigation, however, this conclusion cannot be taken to the micro HEMPT. Influence to the electric potential by the electrons has been removed from the calculation in order to study only the movement of the electrons in external electric and magnetic fields.

## G. Model of a plasma near the cusp

To actually investigate the shape of the potential drop, plasma with an initial density of $1 \cdot 10^{16}$ particles per cubic meter is inserted in the previous model, which creates plasma potential. This model has the same domain size, static magnetic field and cathode electron source as the cusp electron model. The potential on the left side of the model is again set to 166.7 V, yet this time there is no pre-defined potential drop. The right side of the domain is grounded. The lower side is an open boundary with respect to cylinder coordinates. The upper side is at 2.5 mm radius (surface of metallic parts), while for the particles the discharge chamber radius is kept through a particle absorber for all particles with a position $r >= 1.5$ mm. The void in between represents the dielectric material of the discharge chamber walls. The surface charge accumulation described in chapter II E, Eq. 14 is accounted for by replacing the absorbed electrons and ions with immobile ones at

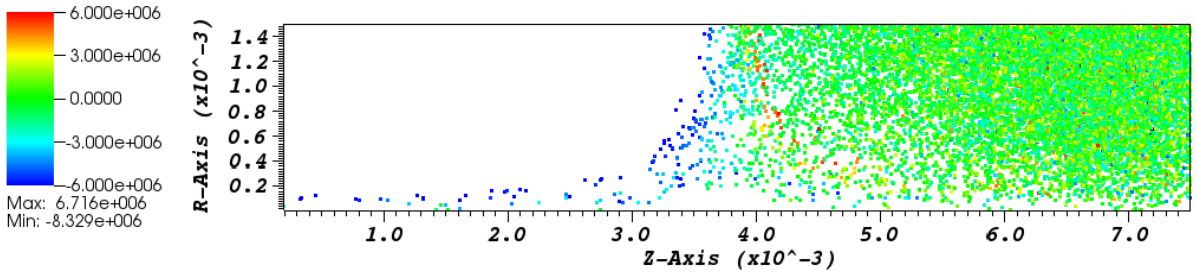


**Figure 8. Distribution of the macro-electrons after movement in the electric and magnetic field of a cusp for $3 \cdot 10^{-9}$s. Phi component of the velocity, m/s, is shown by coloring.**

$r = 1.5$ mm. While for the ions this does not concur with the real neutralization reaction, for the charge the net effect remains the same when ions are added instead of electrons removed from the surface. Like the previous one, this model is incomplete on purpose. It does not include ionization processes. Its purpose is to focus solely on the movement of a given electron and ion distribution in the external and self-generated fields. Later works may go back to this model and see which changes the ionization process made.

# IV. Results

## A. Neutral gas distribution

The results show a pressure drop of 30 Pa near the anode to 4 Pa near the discharge chamber exit (Fig. 3).

## B. Magnetic field

The $B_r$ component has its maximum absolute value near the cusps. The $B_z$ component has its maximum absolute value between the cusps. Both $B_r$ and $B_z$ component are zero near the $z$-position of the cusp at $r$=0 (Fig. 4).

## C. Electron reflection, analytic

The results are plotted in figure 5 a), with a color scheme representing the trapping probabilities. There are almost ellipsoid shaped areas with high trapping probabilities near the two cusps and their maximum is at $r = 0$. There are two other non-separated areas with high probability on the outside near the discharge chamber exit. The one closer to the exit is bow-shaped. They are less symmetric than the ones near the cusps due to the more complex magnetic field geometry compared to the cusp area. Everywhere else the trapping probability is almost zero. Inside the discharge chamber 4.7 of the electrons are trapped.

## D. Electron reflection, numeric

At the last time step, all electrons except ones in a few regions have been absorbed by the boundaries. These regions are each at the two cusps, and one bow-shaped at the cusp exit, and another cloud further away from that exit (Fig. 5 b) ). These regions fit very well with the regions of highest trapping probability from the analytical. Yet near the maximums of the trapping probability the electron density is rather low. This can be explained by the fact that the electrons move the fastest through this region as they oscillate between their mirror points. They can move significant distance from their initial positions before they are reflected, and they accumulate near the mirror points due to their slow speed there. After $1 \cdot 10^{-7}$ s, from the 65000 macro-electrons that originated in the discharge chamber, 3000 - these are 4.6% - are left. Their number is still decreasing at $1 \cdot 10^{-7}$ s, however, the loss rate appears to be negligible at that point.

## E. Fluid plasma model

The result for the ion density at the last time step of the simulation has a maximum of $1.3 \cdot 10^{17}$ particles per cubic meter (Fig. 6 a) , so it has at least in one region increased since the beginning of the simulation.

There are two maxima: one between the two cusps, and one at the anode. The ionization rate has a similar structure like the ion density (Fig. 6 b). As expected, the distribution of the electron temperature (Fig. 6 c) follows the magnetic field lines (chapter II E, Eq. 12). The electric potential drops rather smoothly in steps near the cups (Fig. 6 d). It is assumed that the reason for the drop is due to the fact that the electrons are hindered in passing the cusps by their radial field, while the ions, which are barely effected by the magnetic field, can pass them freely. This can be seen in the $z$-component of the electron current (Fig. 7 a), which is zero near the cusps. On the other hand, the $r$-component of the electron current is very strong near the cusps (Fig. 7 b). The electrons are following the magnetic field lines. However, it should not be forgotten that here the magnetic mirror effect is not accounted for. It can be assumed, that through the mirror effect the current into positive and negative $r$-direction equals out over time. In conclusion, much less electrons might be lost at the cusps than in this fluid simulation. Indeed, particle-in-cell simulation for a normal sized HEMPT has shown for low $r$-postions a higher electron and ion density near the cusps than in between them.[21] The phi-component of the electron current shows strong regions of $E \times B$ drift near the cusps, but also in tails into the $z$-direction away from them towards the anode (Fig. 7 c). It must be taken into account that these are the conservative currents, so the electrons actually move into the opposite direction than implied by the color scheme.

### F. Cusp electron model

As expected, a few electrons have passed the cups in the $z$-direction (Fig. 8). The ones which have passed are close to the $z$-axis; practically none have high $r$-values. Remarkably, most of them have a speed in the phi-direction, forming a ring-current. Apparently the electrons keep their momentum into the phi-direction (which they got through E $\times$ B drift near the cusp) as they move to the left, forming a tail of ring current that has its origin near the cusps. This concurs with the ring current tail seen in the fluid simulation (chapter IV E). On the right side of the cusp is a bow-shaped region with an opposite directed ring-current.

### G. Cusp plasma model

A plot of the different particle types shows that after $2 \cdot 10^{-9}$ s the positive potential has already started to drain the electrons on the left side of the cusp (Fig. 9 a). Like in the "cusp electron model" the cusps acts as a barrier for most of the cathode electrons. For the electrons of the initial plasma, the cusp acts as a barrier as well. The ions are still unaffected after such a short time. A potential step is clearly visible (Fig. 10 a). After $8 \cdot 10^{-8}$ s the side left from the cusp is almost a void of electrons (Fig. 9 b). On the right side the cathode electrons have become a significant fraction of the overall electrons. (Fig. 10 b). Also on the right side, a significant negative surface charge has built up. Supposedly many electrons right to the cusp, following the magnetic field lines (Fig. 4), impact on the surface. This should be especially the case for the cathode electrons, who originate near the right boundary of the domain, and therefore most of "their" field lines end on the surface. After $4 \cdot 10^{-7}$ s the number of ions has greatly diminished, by flux to the right side due to the potential gradient, as well as towards the radial direction (Fig. 9 c). As expected, the flow of the ions is not hindered by the cusp. Due to the overall decreased plasma density, the potential is now almost completely determined by the fixed potential on the left wall of the domain, as well as the surface charges that had built up over time (Fig. 10 c). The lack of electron and ion generation through ionization means increasing diversion from real plasma as the time proceeds. Therefore the results of the time $8 \cdot 10^{-8}$ s are believed to be more useful that the ones of $4 \cdot 10^{-7}$ s. Also when a system has reached steady state, the cathode and anode electron-current is equal, which is not given here. Nevertheless the model indicates that different electron density and velocity directions at opposing sides of the cusp might play a significant role in the surface charge accumulation.

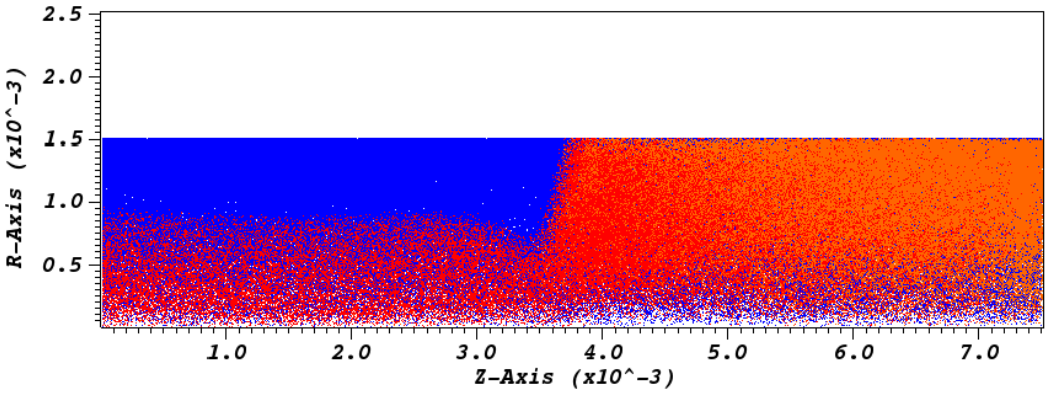


(a)

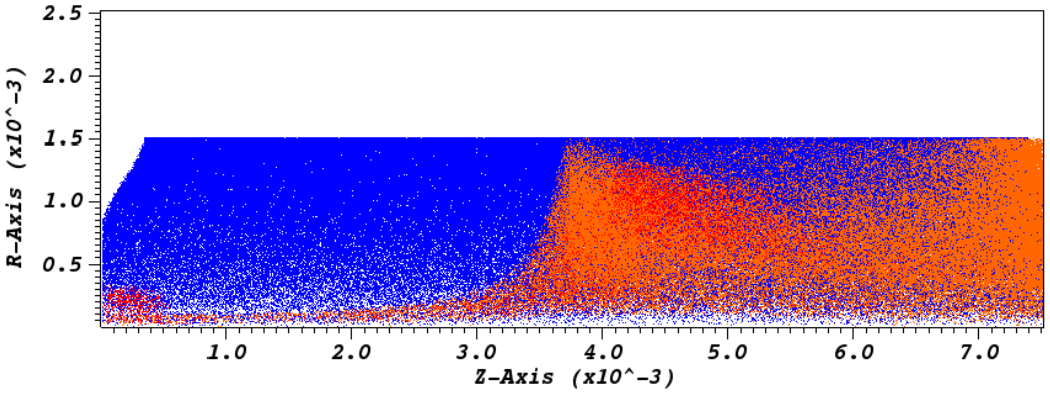


(b)

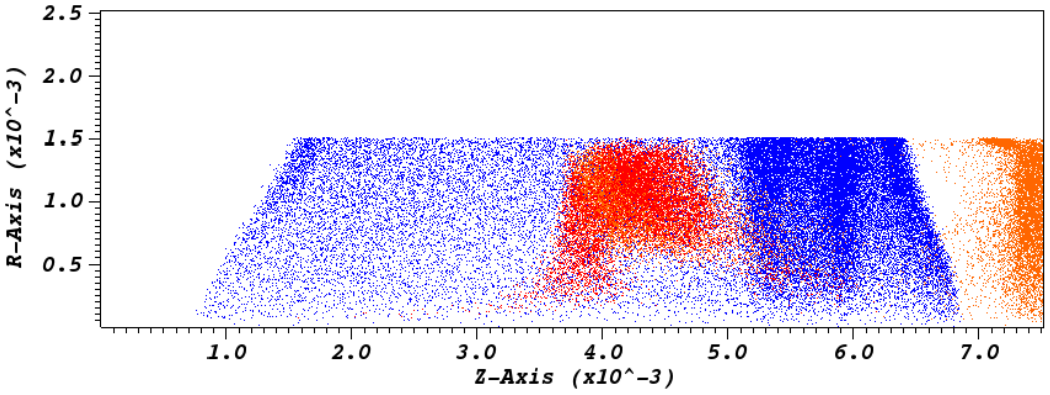


(c)

**Figure 9. Distribution of the macro-electrons and macro-ions after a) $2 \cdot 10^{-9}$ s, b) $8 \cdot 10^{-8}$ s and c) $4 \cdot 10^{-7}$ s. Initial ions blue, initial electrons red, cathode electrons orange.**

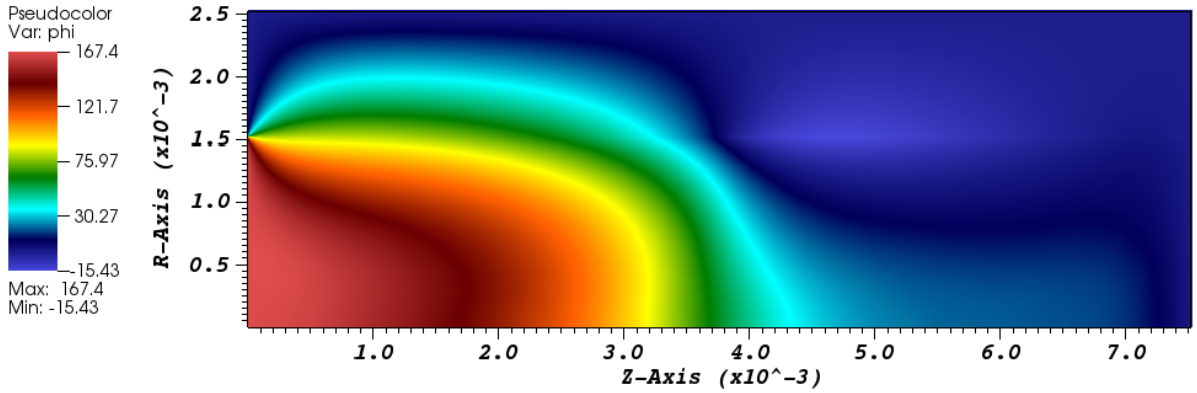


(a)

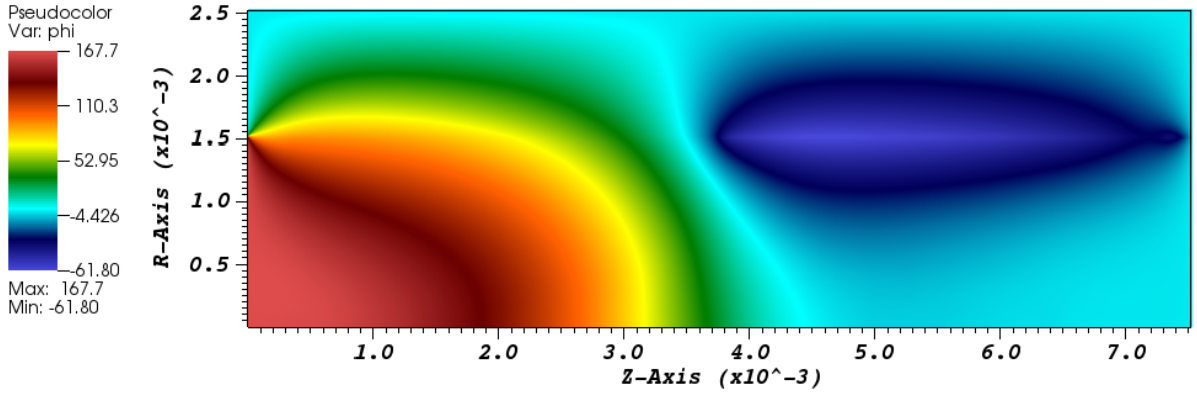


(b)

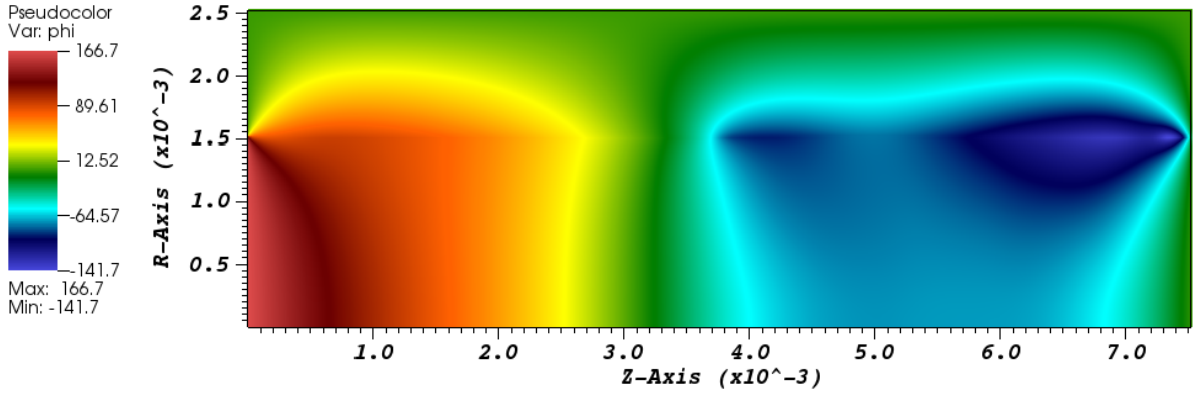


(c)

**Figure 10. Electric potential in V after a)** $2 \cdot 10^{-9}$ **s, b)** $8 \cdot 10^{-8}$ **s and c)** $4 \cdot 10^{-7}$ **s.**

## V. Conclusion

Some basic principals of single particle motion, particle in cell method and its application to modeling the micro HEMP-Thruster have been demonstrated. An analytic method to investigate electron confinement for the simple case of no electric fields has been developed. A particle in cell simulation validates this method and vice versa. A relatively simple fluid plasma simulation of the micro HEMP-Thruster has been performed, by use of a finite volumina element simulation for the neutral gas distribution. Advantages and disadvantages of fluid simulation for this type of thruster have been shown. Movement of electrons originating from the cathode (neutralizer) in the environment of a magnetic cusp with an external electric field has been simulated by use of particles. Furthermore, a simplified particle in cell plasma simulation shows the formation of a step in the plasma potential near the cusp. Improvement of the realism of this model is required to confirm this.

## Acknowledgments

The authors acknowledge fruitful discussions with Thomas Trottenberg, Dennis Weise and Franz Hey. Also acknowledged is Tech-X staff member Sudhakar Mahalingam, who's experience in particle in cell codes provided a great resource in the development of our own models.

## References

[1] Kornfeld, G., Koch, N., and Harmann, H., " New Performance and Reliability Results of the Thales HEMP Thruster", Proceedings of the 4th International Spacecraft Propulsion Conference (ESA SP-555). 2-9 June, 2004.

[2] Kornfeld, G. ; Thales Electron Devices GmbH, Ulm, Germany ; Koch, N. ; Coustou, G., "The highly efficient multistage plasma (HEMP) thruster, a new electric propulsion concept derived from tube technology", 4th IEEE International Conference on Vacuum Electronics, 2003.

[3] A. Genovese, A. Lazurenko, N. Koch, S. Weis, M. Schirra, B. van Reijen, J. Haderspeck, and P. Holtmann, "Endurance Testing of HEMPT-based Ion Propulsion Modules for SmallGEO", 32nd International Electric Propulsion Conference, Wiesbaden, Germany September 11 15, 2011.

[4] Wirz, R.E. ; Anderson, J.R. ; Goebel, D.M. ; Katz, I., "Decel Grid Effects on Ion Thruster Grid Erosion", Plasma Science, IEEE Transactions on (Volume:36 , Issue: 5 ).

[5] N. Koch, M. Schirra, S. Weis, A. Lazurenko, B. van Reijen, J. Haderspeck, A. Genovese, P. Holtmann, R. Schneider, K. Matyash, and O. Kalentyev, "The HEMPT Concept - A Survey on Theoretical Considerations and Experimental Evidences", 32nd International Electric Propulsion Conference, Wiesbaden, Germany September 11 15, 2011.

[6] Andreas Keller, Peter Kőhler, Davar Feili, Marcel Berger, Claus Braxmaier, Dennis Weise, Ulrich Johann, "Feasibility of a down-scaled HEMP-Thruster", IEPC-2011-138.

[7] Chet Nieter, John R. Cary, "VORPAL: a versatile plasma simulation code", Journal of Computational Physics 196 (2004) 448473.

[8] Adrian Down, "Single Particle Motion in E and B Fields", January 24, 2007.

[9] Ju Li, "Notes on Adiabatic Invariants", May 25 1998.

[10] Eyvind Niklasson, "Modeling the Path of a Charged Particle in a Magnetic Mirror", Research Academy for Young Scientists July 11, 2012.

[11] Birdsall, C.K., "Particle-in-cell charged-particle simulations, plus Monte Carlo collisions with neutral atoms, PIC-MCC", Plasma Science, IEEE Transactions on (Volume:19 , Issue: 2 ).

[12] Hideo Okuda, "Nonphysical noises and instabilities in plasma simulation due to a spatial grid", Journal of Computational Physics 10 (3): 475 (1972).

[13] M. M. Turner, "On the accuracy of particle-in-cell simulations with Monte Carlo collisions", National Centre for Plasma Science and Technology and School of Physical Sciences, Dublin City University, Dublin, Ireland.

[14] Skeel, R. D., "Variable Step Size Detabilizes the Stmer/Leapfrog/Verlet Method", BIT Numerical Mathematics, Vol. 33, 1993, pp. 172-175.

[15] Igor V Sokolov, "High-order field interpolation in a charge-conserving numerical scheme for particle-in-cell simulations", Technical Report arXiv:1101.0809, Jan 2011.

[16] H C Kim, F Iza, S S Yang, M Radmilović-Radjenović and J K Lee, "Particle and fluid simulations of low-temperature plasma discharges: benchmarks and kinetic effects", J. Phys. D: Appl. Phys. 38 (2005) R283R301.

[17] G J M Hagelaar, "Modelling electron transport in magnetized low-temperature discharge plasmas", Plasma Sources Sci. Technol. 16 (2007).

[18] G. J. M. Hagelaar and L. C. Pitchford, "Solving the Boltzmann equation to obtain electron transport coefficients and rate coefficients for fluid models ", Plasma Sci. Technol., 14:722733, 2005.

[19] Van Norton, Roger, "The motion of a charged particle near a zero field point" New York: New York University: Courant Institute of Mathematical Sciences,. 1961.

[20] K. Matyash, O. Kalentev, R. Schneider,F. Taccogna, N. Koch and M. Schirra, "Kinetic simulation of the stationary HEMP thruster including the nearfield plume region" IEPC-2009-110

[21] R. Schneider, K. Matyash, O. Kalentev, F. Taccogna, N. Koch, and M. Schirra, "Particle-in-Cell Simulations for Ion Thrusters", Contrib. Plasma Phys. 49, No. 9

*Computer Software*
VSim (including VORPAL engine), Ver. 6.2.2, Tech-X Corp
COMSOL Multiphysics, Ver. 4.3b, COMSOL Group
RhoPimpleFoam, Ver. 2.1.1, OpenFOAM Foundation